Energy 230 (2021) 120785

Contents lists available at ScienceDirect

Energy

journal homepage: www.elsevier.com/locate/energy

Development of thermo-electrical model of photovoltaic panel under hot-spot conditions with experimental validation

Filip Grubišić Čabo [a, b], Ivo Marinić-Kragić [a], Tonko Garma [a], Sandro Nižetić [a, *]

[a] University of Split, FESB, Rudjera Boskovica 32, 21000, Split, Croatia
[b] Include R&D Department, Don Frane Bulica 183a, 21210, Solin, Croatia

ARTICLE INFO

Article history:
Received 11 March 2021
Received in revised form
22 April 2021
Accepted 23 April 2021
Available online 13 May 2021

Keywords:
Photovoltaics
Hot-spot
Solar energy
Experimental
Efficiency
Renewables

ABSTRACT

This work was focused on development of thermo-electrical numerical model for circumstance of free-standing photovoltaic (PV) panel exposed to hot-spot effect. The model was developed for partial hot-spot situation and for serial cell connection. The developed 3D model uses a novel approach via two-way coupling of thermal and electrical models. The model was experimentally validated for geographical location of Mediterranean climate, using the readings from temperature sensors, as well as thermal imaging data. The comparison of results between measured and simulated values were shown to be well matched, with deviation not more than 1.5 °C. The model could be useful for optimization of the bypass diodes and better understanding of hot-spot coupled with other thermal effects. Also, the model can be used for examinations in the case of building integrated photovoltaics (BIPV), since hot-spot effects could be utilized as additional heat sources that could be properly managed. The effect of temperature non-uniformity could be also examined with herein proposed modelling approach and which is beneficial in the case of cooled PV panels.

1. Introduction

Photovoltaic capacities present an important source of energy with respect to the general energy transition goals where by now, over 580 GWp [1] of global photovoltaic capacities have been commissioned, with an estimate to reach about 8000 GWp by 2050 [2]. Previous estimates indicate global importance of the PV technologies where currently mainly silicon based technology (both mono and poly crystalline) are the most represented on the market [3]. Other technologics with market potential, such as Perovskite or organic photovoltaic cells are still experiencing specific development barriers towards potential wide market implementation [4]. In order to successfully achieve goals towards the transition to renewable energy sources, and to fulfil environmental, safety and reliability criteria, photovoltaic (PV) panels require extensive laboratory and field tests [5]. One such safety and reliability criteria is influence of hot-spot effect. The phenomenon known as hot-spot is also affecting the performance of the PV panels [6], so corresponding measurements and modelling of mentioned effect is important in order to gain insights and to prevent performance degradation. According to the exisiting research findings, the PV panel will experience hot-spot in two different cases. The first case is a reverse bias intentionally connected to solar cell [7]. First case investigations are obtained in laboratory conditions to study extreme and rare overheating and its influence on PV panel's performance. This work deals with the second case of the hot-spot. Namely, if a solar cell generates less current than the string current of the panel, it will develop hot-spot. This second case of hot-spot can occur in the actual in-situ environment and research related to it may be of more interest to a PV community oriented towards the practical aspects of the PV systems [8]. Assuming an accurate connection scheme within the PV panel, aforementioned phenomenon occures on solar cells which are shaded or damaged to some extent. Typical examples of shading, other than clouds or objects surrounding the PV panel, are bird droppings and dust [9].

Partially or fully covered cells reduce the current through fully functional cells. Consequently, healthy cells are forced to operate in higher voltage regime, resulting in switching the shaded cell in reverse bias mode. In extreme cases, the previous can lead to the temperatures higher than 150 °C, which is above the long-term maximum operating temperature of the cell encapsulants for commercial panels [10]. The heating effect is even more

* Corresponding author. University of Split, Rudjera Boškovića 32, 21000, Split, Croatia.
E-mail address: snizetic@fesb.hr (S. Nižetić).

https://doi.org/10.1016/j.energy.2021.120785
0360-5442/

pronounced in case of sufficiently large shade [11]. This can result in front side cracking, solder melting and general degradation of the panel's electric properties [11]. Since previously described damages are highly non-desirable, various preventive mechanisms are applied. Integration of bypass diodes in the cell interconnection circuit creates alternative current path and relaxes thermal load on the shaded cell. The number of bypass diodes is limited by both technical and economic aspects, thus intense hot-spots usually result in bypassing not only shaded cell, but also the rest of the string [10,12].

Different approaches have been used in order to investigate theoretical background and practical influence of hot-spots and related phenomena on solar cell operation. Fundamentals of hot-spot heating are reported in Refs. [10,11]. The same research group extend the investigation towards hot-spot induced reverse biased conditions solar cell operation, measuring reverse bias I–V characteristics and critical reverse bias voltage [8]. Avalanche breakdown due to etch-pits is demonstrated in Ref. [8], resulting in method for analysing avalanche breakdown based on electron-beam-induced current. Extensive numerical models dealing with shaded cells are reported in Refs. [13,14], while work [15] reports PV modules hot-spot susceptibility. Influence of shading was examined in Ref. [16] with respect to PV cell electrical properties. More recent work [10], analysed PV array configurations under several partial shading conditions including series, parallel, 11 bridge-linked or total-cross-tied configurations. The study dealing with effect of partial shading has been reported in Ref. [17] where authors varied solar irradiance levels for PV panels (90 Wp). In the same work beside the deterioration of the performance the long-term degradation was also noticed. Sharma et al. [18] focused their research to maximum power from partially shaded PV arrays using shunt-series compensation. In mentioned investigation, a current-compensating converter was connected in shunt with each panel, and a voltage-compensating converter was connected in series with each string. The aforementioned paper is complemented by Deshkar et al. [19] proposing genetic algorithm for maximum power extraction algorithm. Work published in Ref. [20] reported novel maximum power point tracking techniques for PV systems exposed to partial shading based on Flower Pollination Algorithm including the randomness in every iteration. Contrary, more recent study was focused on maximum power extraction from partially shaded PV systems [21,22]. While traditional techniques were limited to global peak tracking, authors in Farh et al. [21] developed system that can track peaks of the PV arrays (their sum) and where interleaved boost converter (IBC) was used. A new configurations were proposed in Belhaousas et al. [22] simplifying operation and improving the performance in comparison to the reference Series-Parallel (SP) as well as Total Cross Tied (TCT) configurations. The results indicated that the specific P–V curves exhibit a single peak and which ensured tracking of the MPPT using the simple controller and without need for complex algorithms for control. A certain gap, arising from the fact that detection and assessment of various scenarios of partial shading was not studied as often as other PV-related topics, was overcome by Ma et al. [23]. In the mentioned work the shading strength as well as shading rate were taken to consider various scenarious with respect to the algorithm related to the shading pattern.

Thermal modelling of PV panel is usually performed using thermal and coupled fluid dynamic simulation, since the heat transfer from the PV panel to surrounding fluid is dominant in overall heat transfer. These models are most commonly used when analysing cooling techniques such as forced or natural ventilation, phase change material system, water cooling etc. [24]. An example of a cooling technique with passively air-cooled heat sinks (similar to design used in this study) was analysed in Ref. [25]. The PV panel was located in a ventilated façade, and the cooling element was finned wall on the bottom of the PV panel. The numerical model included both the thermal and the fluid dynamic simulation. In this manuscript, applied passive cooling approach is the one developed in Ref. [26] and further refined in Refs. [27,28]. These papers almost always used coupled thermal and fluid simulation, with exception of [27], where fluid simulation is replaced with analytically calculated convection coefficients. There are many related papers regarding passive cooling [29,30], but the common topic in most is average temperature reduction. A related important metric is temperature uniformity [31], especially important when considering the PV panel with hot-spot. Except with bypass diodes [10], this issue can also be handled by keeping uniform temperature distribution [32] across the cells. For numerical modelling of this situation, the thermal model needs to be coupled with the electric model. Papers which deal with hot-spot modelling and temperature uniformity such as [33] are usually based on electric model with integrated cell-based thermal model. In Ref. [34], a numerical study was performed in which water cooling was used to achieve an uniform cooling with 0.9 °C standard variation on the surface of PV. The numerical model was based on coupling of computational fluid dynamics (CFD), thermal, radiation, and electrical model. Thermal model of PV panel was developed with respect to previous models [27] along with a case with cooling fins added to the back side. Coupling of CFD and thermal model with the radiation model was performed by calculating the incoming solar radiation and then used as a heat source term in the model (one-way coupling). The objective of the electrical circuit modelling was to evaluate output parameters; current, power, and voltage (again one-way coupling). Two-way coupling would include exchange of data during the simulation between the thermal model and the electric model in each time step, as schematically shown in Fig. 1. The interaction includes transfer of calculated temperature from the thermal model to the electrical model, for each cell separately. This is then used as a parameter within the electrical model of the whole PV panel. With addition of the prescribed solar irradiance distribution and the operating voltage, the electrical model can be used to calculate the heat generation for each cell. This data transfer occurs at each simulation time-step within the two-way coupling model.

Up to now, many researchers investigated models of photovoltaic modules from either thermal [35] or electrical aspect [36]. There also exists research which investigates coupled electric and

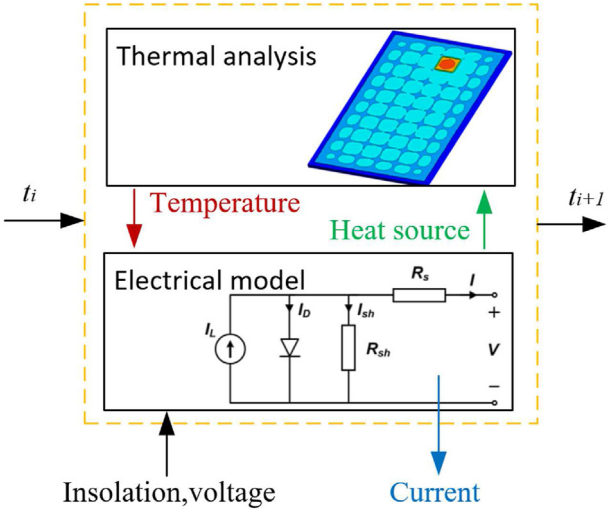

Fig. 1. Two-way coupling model simplified schematic.

thermal models [37]. However, there is a lack of literature regarding two-way coupling between a 3D thermal model and the electrical model.

The main objective in the herein presented study is development of novel two-way coupling of a detailed 3D thermal model with a cell-based electric model. The integrated thermo-electrical model, with two-way coupled hot-spot effect has not yet been adequately covered in existing literature, which presents the main novelty of this work. Especially, this has never been made as an integrated numerical model with experimental validation. Herein proposed interconnected and interdisciplinary approach enables deeper insight in problematics of hot-spot effects and its connection with cooling techniques. More importantly, this enables the analysis of heat transfer effects by additional parameter, hot-spot mitigation and further performance improvement of specific cooling techniques for photovoltaics.

2. Theoretical background

2.1. Electrical model: Hot-spot effect

As mentioned in the introduction section, hot-spot effect manifests itself as a noticeable jump in the PV panel operating temperature (cell temperature in fact). Even though an intense overheating of affected cell appears to be purely macroscopic, its origins are arising from the energetic processes occurring at the PN junction of the shaded cell. In the shaded PN junction, two processes relevant for hot spot are occurring: rise of the PN barrier height and the reduction of the barrier width. While the former phenomenon generates the reduction in carrier mean free path and space charge region expansion (barrier capacity reduction), the latter results in increased probability for carrier tunnelling, i.e. in the case of the extreme shading. If extreme shading and tunnelling does not occur, the total generated power of the rest of the PV module connected in serial connection (n-1 cells), dissipates in one shaded cell. Since power dissipation process occurs in the shaded area it is relatively small in comparison to the rest of the module surface, local overheating is virtually unavoidable. Depending on the current − temperature characteristics, it is possible to distinguish two separate effects, i.e. field emission (Zener breakdown) and impact ionization (avalanche breakdown). In the case of Zener breakdown, as a result of band-gap lowering, current slightly increases with temperature [11]. Contrary, for the avalanche breakdown, increased phonon scattering results in strong current decrease with the increase in temperature [11]. In this case not only shaded cell but also all cells connected to it in series will be flowed by excessive current.

2.2. Modelling approach

Mostly all electrical models of the operational photovoltaic cell are based on Shockley diode equation, as presented in Ref. [38], and later used in Ref. [39] as well as similar studies, respectively

$$I = I_L - I_D\left(e^{\frac{qV+IR_s}{nk_BT}} - 1\right) - \frac{V+IR_s}{R_p}\left(1 + \frac{\alpha}{\left(1-\frac{V+IR_s}{V_{br}}\right)^m}\right) \quad (1)$$

Here, IL is light induced current, given by expression as follows,

$$I_L = \frac{G}{G_0} I_{L0} \cdot A_{cell} \cdot (1 + 0,0006 \cdot (T - 293)), \quad (2)$$

where G is actual solar irradiance, G_0 is solar irradiance at standard testing conditions, I_{L0} is light induced current density at G_0, A_{cell} is the surface of the cell, T is cell temperature. The equation has in itself incorporated the rise in the current as an effect of the temperature increase (0.06% per °C). Mentioned expression can therefore be used to express the amount of current gained by solar irradiance. Note that Eq. (2) has PV cell efficiency indirectly incorporated via the value of I_{L0}. For the second equation member, I_0 is dark saturation current, q is an electron charge, R_s is cell series resistance, n is a diode quality factor and k_B Boltzman constant.

The third equation member is directly related to hot-spot effect, and it is usually omitted when hot-spot is not modelled or taken into account. Here, R_p is cell shunt resistance, α is the fraction of ohmic current (that is involved in avalanche breakdown), V_{br} is the junction breakdown voltage, and m is the avalanche breakdown exponent. The model in this study will only deal in partial hot-spot on a PV cell. It was shown by experimental measurements (thermal imaging) that for partial hot-spots observed in this manuscript bypass diode is not triggered.

Eq. (1) can be solved by numerical iteration, which will give I–V characteristic of a single cell. In order to solve it, a modified Matlab code from Ref. [40] was used, and parameters for single 6″ cell were implemented in the model. I_D is dark saturation current, given by the following equation,

$$I_D = A_{cell} \cdot I_{D0} \cdot 2^{\left(\frac{T-293}{10}\right)} \quad (3)$$

where I_{D0} is dark saturation current measured for typical silicon cell at room temperature. Note that the expression has a temperature dependence integrated into it, in a manner that dark saturation current doubles with each 10 °C increase at lower operating temperatures [41].

Temperature dependency is implemented via the feedback loop from the thermal model and developed in Ansys software, where temperature value is imported from the model (details would be explained in following sections of the manuscript). Series resistance Rs is given by the following equation,

$$R_s = \frac{R_{s0}}{A_{cell}}(1 + \Delta r(T - 293)), \quad (4)$$

where R_{s0} is specific serial ohmic resistance, and Δr is a raise in serial resistance due to increase in the temperature (although this raise is fairly small).

Shunt resistance is given by the expression as follows,

$$R_p = \frac{R_{p0} \cdot e^{\left(\beta\left(\frac{1}{T} - \frac{1}{293}\right)\right)}}{A_{cell}} \quad (5)$$

where R_{p0} is a characteristic shunt resistance for crystalline silicon cell at 20 °C, and β is thermistor temperature constant.

When solving Eq. (1), this will later reflect on the relation of voltage upon the PV cell operating temperature.

The values used in these equations are given in Table 1 [39].

2.3. Thermal model

2.3.1. Principles and governing equations

Thermal model of photovoltaic cell is based on the previous work presented in Ref. [27], where a simplified approach was used. The main heat source in photovoltaic cell is solar irradiance. Other sources, such as thermal radiation from surrounding objects or a convective heat source are practically non-existent, since in large

Table 1
Input values for electrical model.

Parameter	Unit	Value
I_{L0}	A/cm^2	$32.7 \cdot 10^{-3}$
G_0	W/m^2	1000
A_{cell}	cm^2	244
q	C	$1.6 \cdot 10^{-19}$
k_B	J/K	$1.38 \cdot 10^{-23}$
n	–	1.2
R_{s0}	Ωcm^2	0.5
Δr	Ω	0.003819 [41]
R_{p0}	Ωcm^2	1000
I_{D0}	A/cm^2	$5.5 \cdot 10^{-9}$
V_{br}	V	−15
α	–	0.35
m	–	3.8
β	K	−0.07 [11]

majority of cases PV cell is the hottest element in its surrounding. The heat therefore originates from the solar cell, but small extent of it also originates from the front (see Fig. 2) panel surface (predominately glass, or a polymer structure). This extent goes from 1% to 5% of total irradiance, depending of cover properties. Typical properties of most common front side material, silicate glass, can be estimated as follows: transmissivity of around 0.93, reflectivity of around 0.05 and absorptivity of less than 0.02 [42]. Absorptivity is typical for lower wavelengths (UV radiation) for which the glass is not transparent. For simplicity, in future analysis glass will be presumed as non-absorbent material when it comes to regular spectrum of solar irradiance.

Other properties of the materials were taken as follows:

- EVA (Ethylene-Vinyl Acetate – commonly used binder in photovoltaic industry) was treated as fully cured material of homogenous thermal properties,
- Silicon cell was treated as completely opaque for complete solar spectrum,
- The reflection of the silicon cell, with respect to the anti-reflection coating applied to the cell, was attributed directly to the glass surface. The purpose of mentioned simplification was to enable easier numerical modelling.

Heat dissipation from the cell can be divided into two main components, Q_{front} which represents heat dissipation from the front side, and Q_{back} which represents heat dissipation from the back side. Dissipation from the sides Q_{side}, although taken into account in modelling, is definitively by the order of magnitude lower than that from front or back side.

For steady state, which was analysed in the model (i.e. no change in internal energy), a following thermal equilibrium can be stated, i.e. First law of thermodynamics:

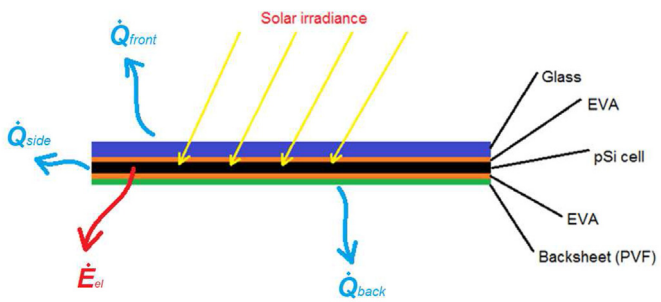

Fig. 2. Material structure and energy flows of PV panel segment.

$$\dot{Q}_{solar} = \dot{Q}_{front} + \dot{Q}_{back} + \dot{Q}_{side} + \dot{E}_{el} \quad (6)$$

Here,

$$\dot{Q}_{solar} = G \cdot A \cdot \tau \cdot a, \quad (7)$$

where G is solar irradiance (a measured value), A is surface area of photovoltaic cell, τ is glass transmissivity and a is absorptivity of silicon cell. Overall coefficient which takes into account both glass transmissivity and cell absorptivity can be estimated at 0.87.

Components Q_{front}, Q_{back}, and Q_{side} each have their convective and radiative component, and their calculation is addressed in the section related to the numerical modelling. On the back side, the convective component is much more dominant, since back side temperature is not significantly different from its surrounding (up to 20 °C of difference). Front side, on the other hand, exchanges the radiative heat with the sky, which has fairly low apparent temperature and thus the heat exchange is much more intensified.

Electrical current E_{el} was calculated via measured values of current and voltage. Current is available from the measurement [27], and voltage is obtained for each cell by solving Eq. (1). The hot-spot induced heating is added into the equation in the manner that the cell, when it switches to reverse bias mode, will generate negative voltage. This voltage, multiplied by current, corresponds with thermal dissipation in each individual cell. Hence, in hot-spot cell, $\dot{E}_{el}$ will actually be negative, and thus result in higher heat accumulation in the cell.

2.3.2. Different hot-spot working regimes

There are two distinct hot-spot working regimes, which need to be assessed when modelling thermo-electrical model with hot-spot effect, namely direct and indirect shadowing. Differences are shown in Fig. 3.

For direct hot-spot effect it is characteristic that there is an obstacle at the surface of the PV panel. This obstacle usually has different reflectivity and absorptivity than the cell itself and since it does not give away electricity, in most cases it additionally heats the PV panel at that specific spot. Indirect hot-spot is produced not by covering effect, but by shadowing of the obstacle that is not positioned at the PV panel surface. This produces the hot-spot effect, but does not additionally heat the front surface.

In numerical modelling, it is crucial to distinguish these two regimes, since this directly influences thermal load on the photovoltaic cell. When it comes to modelling approach, indirect hot-spot is much easier to model, since this does not present any additional heat load and can be modelled only by solar irradiance intensity, G. It is hard to say what is the ratio of direct to indirect hot-spots in-situ, and it would surely be more accurate do develop a model which covers both direct and indirect hot-spot. This however calls for significant model redesign and additional computing time. Hence, for now the model will deal only with indirect hot-spot effects.

2.3.3. Numerical model

The numerical model was developed within ANSYS Fluent [43]. Thermal model was solved using in-build methods, while the coupling with the electrical model was implemented by user-defined functions. A schematic sketch of the modelled energy flows between the PV panel and the surroundings is illustrated in Fig. 4. The main energy flow (largest energy contribution) is related to solar radiation energy that is absorbed by the PV panel. A part of the irradiated energy is directly reflected, but the largest part is absorbed by the relatively thin PV cell layer. Some of the absorbed radiation energy is transferred into useful electrical energy

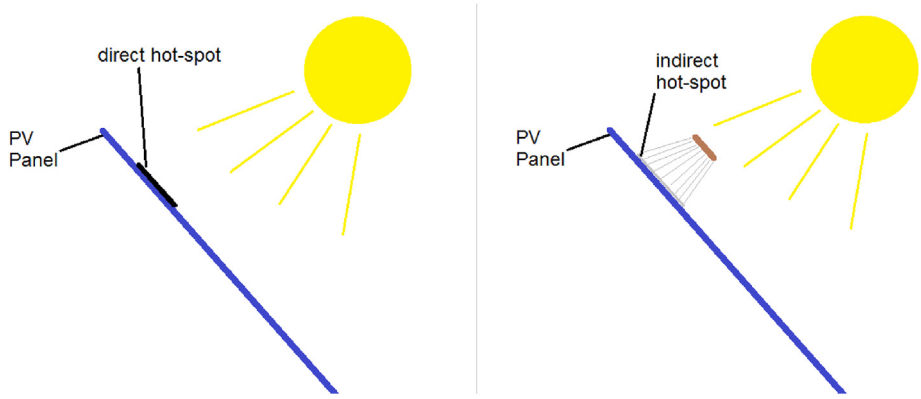

Fig. 3. Two types of hot-spot causation.

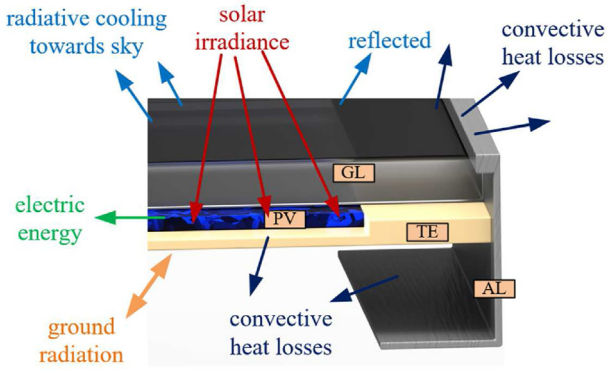

Fig. 4. Simplified representation of the PV panel with main energy flows (GL – glass cover, PV – photovoltaic cell, TE – backboard and AL – aluminium frame).

(photoelectric effect), but the largest part is converted to heat. A smaller part of the irradiance can sometimes be absorbed by the backboard surface from the ground. Since the effective sky temperature is practically always smaller than the PV panel surface temperature, radiative cooling must be modelled on the PV panel upper surface. Among the cooling mechanisms, dominant one is the convective heat transfer from the PV panel to the surrounding air, which is also challenging to model accurately. Within the PV panel layers, heat transfer occurs by pure heat conduction. For each control volume, the sum of all input energy flows must be equal to the sum of all output energy flows in the steady-state conditions.

The main problem with the naturally ventilated system is high dependence of the PV panel placement and the wind flow conditions [44] with respect to the convective heat transfer. The important parameters are wind velocity, air temperature, turbulenece, geometry of the panel elements, surrounding surfaces, supporting structure, etc. The most used modelling approach for analysis of the convective heat transfer is via CFD since reasonable results, with sufficient accuracy can be ensured.

In this study, convection coefficients were used, which were obtained by experimentally validated CFD model in Ref. [27]. As for radiative cooling, several relatively accurate radiative cooling models exist [45]. In this study radiative cooling is not dominant, so simple model can be used. The selected model was the external radiation boundary condition according to ANSYS Fluent [43], which is based on the grey-body expression discretized on individual surface element. On each surface, appropriate emissivity coefficient and surrounding apparent temperature is applied. The energy equation used in the 3D thermal model:

$$\rho\frac{\partial h}{\partial t}=\frac{\partial}{\partial x_j}\left[k\frac{\partial T}{\partial x_j}\right]+S_h \tag{8}$$

where ρ is density, h is enthalpy; k thermal conductivity; T is the temperature; S_h is the volumetric heat source and which is equivalent uniform heat flux in PV cell and electric model heat transfer. The volumetric heat source was defined only at the PV cell by:

$$S_{h,cell}=\dot{Q}_{solar,cell}(G_{cell})+\dot{E}_{el}(T_{cell},G_{cell},\ I_m) \tag{9}$$

where T_{cell} and G_{cell} are cell-averaged temperature (K) and insolation (W/m^2) respectively, and I_m is measured current. In a general case, each cell has a different volumetric heat source allocated to it. The solar absorption was calculated by (7) and the electric power was calculated using (1)-(6). These expressions were implemented using a user defined function. Solar irradiance was selected differently for each cell depending on the specific test-case (hot-spot affected cell has lower solar irradiance due to shadowing). The temperature was calculated during the simulation time. This includes a two-way coupling of the electrical model with the 3D thermal model. In each computational time-step, the temperature field is updated based on heat source from the previous time-step. At the end of each time step, the temperature field is used to calculate the average temperature of each cell T_{cell}, which is an input to the electrical model. Based on T_{cell} and G_{cell} for each cell, the electric circuit with all 60 cells is simulated. Depending on the case, overall current or voltage can be specified. Then, by solving the electric model, electric power of each cell is obtained. This electric power acts as a heat sink in all cells, except for the cells with hot-spot effect, where it acts as a heat source (because of its negative voltage). This process is repeated for all computational time-steps until convergence. This is achieved when temperature, electric current and voltage change less than 0.1% between two subsequent iterations.

The computational domain was made by multiple solid regions, such as: backboard, PV cell, glass cover and aluminium frame. In some cases, aluminium fins were added in addition to the previous regions. The regions have the sam temperature as interface (i.e. they are thermally coupled). The Fig. 5a and Fig. 5b present the modelled solid regions and the mesh on two PV panel cross-sections.

The main properties affecting the heat transfer are specified in the Table 2, where selected values were used for each computational domain.

The majority of the regions were discretized using tetrahedrons. The discretization of the PV cell was provided by using a hexahedral

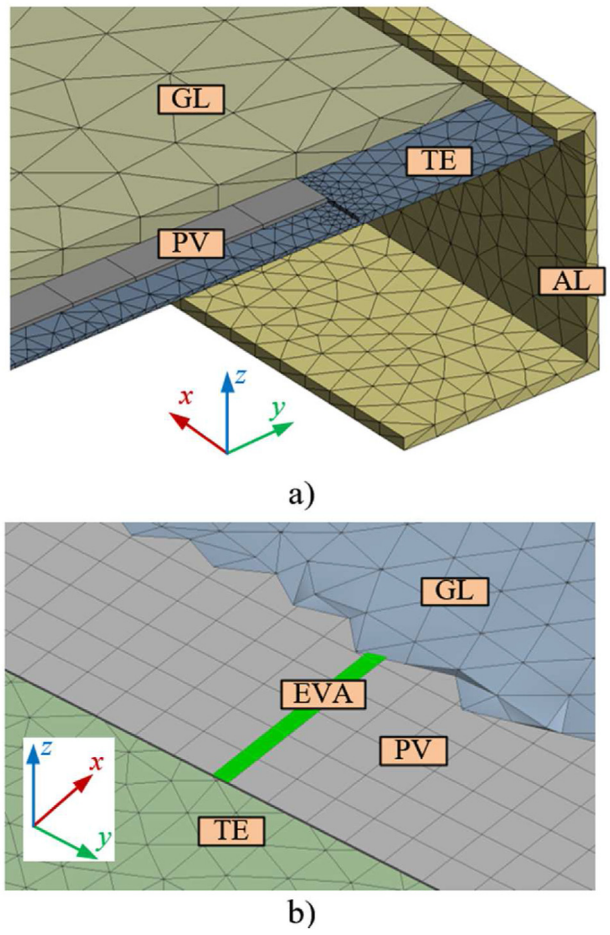

Fig. 5. The computational solid regions for PV panel (GL – glass cover, PV –cell (EVA– insulation/isolation between cells), TE – backboard and AL – aluminium frame): a) section near aluminium frame and b) section near the PV panel centre.

mesh due to simple shape, Table 3. It is important to note that the isolation layer between the cells (Fig. 5) is also a part of the same computational domain, however the thickness of the local element size is such that it is equal to the thickness of the isolation layer.

2.4. Model constraints – bypassing bypass diode

Photovoltaic panel is a commercial product which enables cost-effective conversion of solar irradiance to electricity. Typical panel is silicon based, polycrystalline one string module [3]. For a typical 6″ cell, which is currently most commonly used, this gives approximately 8 Amps DC current (for Isc) and approximately 0.7 V (for V_{OC}) for each cell connected in series. Common commercial solution in photovoltaic technology is full serial connection. Presumably, this is because of Joule heat losses, thus most PV module designs go for serpentine shaped solution. This enables easier application of bypass diodes in the system. The typical setup is presented in Fig. 6.

The purpose of bypass diodes at this stage is to enable bypassing of the whole string for cases when the hot-spot effect induces excessive resistance in a cell. As mentioned earlier, this resistance leads to drastic overheating of the single cell, and thus can cause damage [10]. For a case of significant hot-spot, reverse bias voltage generated by the PV string will appear on the bypass diode terminals and switch it from reverse bias to forward bias operation regime. As a result, net current will gain alternative parallel path characterized by significantly lower resistance. Consequently, current generated by the remaining cells will flow through the bypass diode while bypassed string section will be short-circuited, i.e. disconnected. On the other hand, and as a direct consequence of the mentioned effect all healthy cells in the string protected by bypass diodes will be bridged and they would not contribute to net energy gain. It is also too expensive to install dedicated bypass diode for each cell, so an economical aspect needs to be taken into account: fewer bypass diodes mean cheaper module, but chance of fatal hot-spot effect increases drastically and a portion of energy from healthy cells is lost with bypassing.

Bypass diodes are installed in a manner that they will not activate for minor hot-spot effects. The reason is simple - it is better to gain additional energy from one string with one slightly heated cell, than to lose all the energy from that string in order to fully protect the cells. This means that, for smaller hot spot effects, bypass diodes can be removed from the model, since bypass diodes will not be activated either way. This further enables modelling of minor hot-spot effects without the need to take bypass diodes into account.

Table 3
Mesh type elements and their number per subdomain.

Subdomain	Number of elements	Type
PV cell	17,069	Hexahedral
Backboard	106,139	Tetrahedrons
Glass	105,070	Tetrahedrons
Aluminium	22,855	Tetrahedrons

3. Experimental data validation

3.1. Thermal imaging

Although the radiated energy covers entire wavelength/frequency spectrum [11], IR thermography is limited to the infrared range, meaning wave lengths roughly from 800 nm up to 14 μm. Furthermore, taking into account the atmospheric transmissivity for IR radiation [11], one is practically limited to two subdomains ranging from 3 to 5 μm and 8–14 μm. Virtually ideal atmospheric transmissivity for IR radiation suggests these domains as natural choice for IR camera operation. According to Stefan-Boltzmann's Law [12] ideal black body can be defined, as a body whose emitted radiation will depend on absolute temperature only.

Radiation detected by IR camera consists not only of self-emitted radiation but also reflected radiation originating from

Table 2
The main properties used in the modelling.

Material	Density [kg/m^3]	Thermal conductivity [W/mK]	Heat capacity [J/kgK]	Layer thickness [mm]
PV cell	1000	150	700	0.5
EVA	930	0.23	850	0.5
Backboard	800	0.35	800	0.5–1.0
Glass	2530	0.8	800	3
Aluminium	2719	202.4	871	2

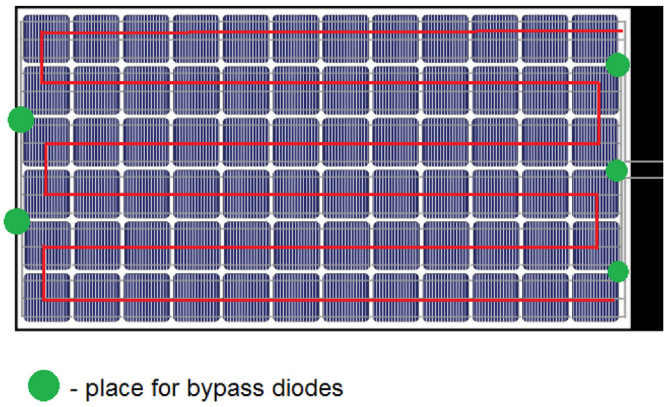

Fig. 6. Placement of bypass diodes on typical photovoltaic panel.

environment. Moreover, atmosphere can attenuate or amplify the existing radiation [13]. The corresponding thermograph compensation consists of introducing so called object parameters, namely, emission factor ε, ambient temperature and environment temperature. Contrary to environment temperature, measuring other two parameters requires more sophisticated approaches as well as theoretical understanding of both parameters. The term ambient temperature refers to the apparent temperature originated from the energy sourced from the environment and reflected from the object of interest. When performing in-situ field measurements, ambient temperature is obtained by multi-planar mirror, cancelling stochastic noise sources.

Emissivity factor of the object of interest also has to be determined since datasheets contain general data [1] and, hence, can be used only for orientation. The procedure for this step varies depending on material constituting the object that is analysed. In the case of solar cells, material is quartz glass with data sheet emissivity of roughly 0.85 [46]. Material system with relatively low emissivity will be an excellent reflector, but rather poor emitter, making the IR thermography measurements challenging and time consuming.

In the setup used for the purpose of this research, surface temperature is obtained using Flir T 335 IR camera. The aforementioned system applies matrix of the uncooled microbolometers (thermal sensitivity 0.05 °C at 30 °C). IR-based results are compared to data generated from thermocouple readings. Before obtaining reliable IR data, it is necessary to input the environmental parameters. Namely, without accurate information considering ambient temperature, the reflected temperature, and the relative humidity, IR data will contain systematic error. Moreover, due to fact that glass is not transparent for the FLIR T335 wavelength regime (7.5–13 μm, IR range), the camera visualizes the apparent temperature distribution of the glass cover and indirectly the heat distribution of the underlying PV panel. Considering glass surface reflections, the IR measurements include various obstacles arising from the heat footprint of the surrounding objects and consecutive misinterpretations. In order to reduce this effect, IR camera position is defined based on minimal reflection criterion. The fulfilment of the criterion is verified by usage of well defined emissivity factor ($\varepsilon = 0.95$) markers on both PV panel sides. The thermography-based data were verified with readings gained from thermocouples. Only negligible offset has been detected, proving the validity of the IR measurements. In addition to the raw thermographs, off-line post processing has been done. This approach enables conversion of the 2D thermograph to temperature vs. position curve graphs that can be obtained for any line arbitrarily selected along the PV module surface.

3.2. In situ conventional measurements

In-situ measurements are explained in detail in Ref. [27]. For easier understanding, main measuring information will be given here, while details can be obtained from Ref. [27]. The measuring setup consisted of 2 sets of 2 × 260Wp polycrystalline silicon panels, where one set of panels used a passive fin based technique on the back side, Fig. 7.

Overally, 16 thermocouples and 8 capacitive sensors were used for measuring temperature, one anemometer was used for measuring air velocity. Two custom made measuring setups were used for measurement of current and voltage for a resistor of 1000 Ohms connected to each system separately. One pyranometer, co-planar to the panels' front surface, was used for measurement of solar irradiance. All measurements were taken for a significant period of time (from June to October, Northern hemisphere), at least 8 h a day and in an interval of 1 s. The most interesting data for this paper are given by thermocouples positioned on front sides of the panels, and also for several thermocouples that are positioned at the back side of the panels. These measurements will be used to validate the model.

As for the input parameters, air temperature, solar irradiance, voltage and current were implemented into the model. Mentioned data were correlated with the thermal imaging data. Because of simplicity, the numerical model consists only of one panel, which is then adjoined with additional panel, thus forming a set. Panels used in the experiment are commercial panels, whose properties are given in Table 4.

4. Model parameters and results

4.1. Case 1 – single hot-spot affected cell

Parameters of the model were determined for specific measurement for which thermal imaging was made (July 28, 2017 [31]). This way, it could be identified which cell is in the hot-spot regime, and this can then be imported into the model. Both systems A and B were used for parameter determination. Thermal imaging showed a characteristic hot-spot effect which is a result of thermocouple marking label. This is shown in Fig. 8.

When analysing area of the shadow on original image, it was deduced that amount of partial shading on a reverse biased cell is 10–15%. When this was implemented into electrical model, by means of reducing the solar irradiance of hot-spot cell for 10%, *U–I* curves were gained which is presented in Fig. 9.

In Fig. 9, it can be noted that two panels are separately calculated and then joined together in the series. It can also be seen that

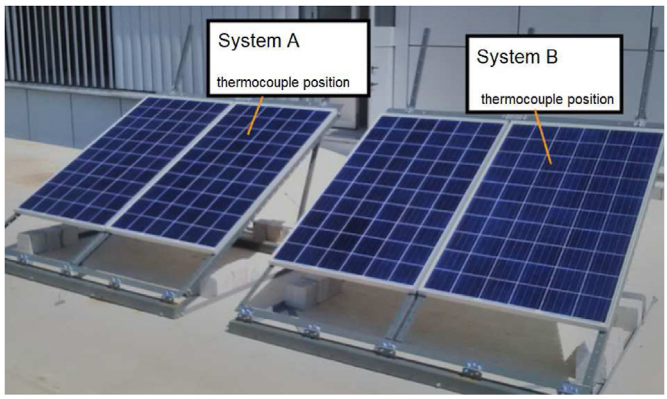

Fig. 7. In-situ experimental setup.

Table 4
Photovoltaic module properties.

Rated Max. Power	P_{max}	260 Wp ± 2%
Open circuit voltage	V_{oc}	36.69 V
Short circuit current	IS_c	8.75 A
NOCT	T_{noct}	45 °C + - 2 °C
Dimensions	mm	1640 × 990 x 34

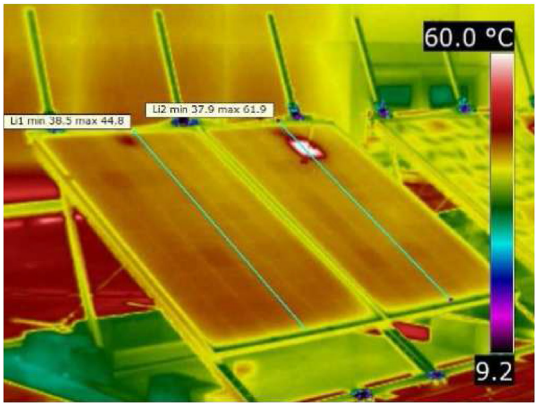

Fig. 8. Thermal imaging of System A.

working point (which is measured in experiment) lies near the *U–I* curve. When placed in the model, where each cell is modelled as a separated heat source and coupled with electrical model, the following is achieved and presented in Fig. 10.

Qualitative numerical and experimental results look promising. On the other hand, quantitative results are of more interest since their matching can verify model's accuracy and enable further testing. Graphs in Fig. 11 show the comparison of quantitative results and their deviation, while lines on graphs correspond with lines in Fig. 8.

Two issues arise from Fig. 11. Namely, as it could be expected, exact quantitative matching of thermal imaging throughout the photovoltaic module length could not be achieved due to general constraint of thermal imaging. The exact emissivity of frontal glass cover cannot be fully defined, and reflection of solar irradiance at the thermal camera cannot be accurately predicted. Second issue is related to front side thermocouple, which again cannot accurately measure front side temperature, because of direct solar irradiance which is hitting the thermocouple. Previously mentioned issues cannot be overcome. Nevertheless, two additional thermocouples positioned on the back side, along with thermal imaging on the back side, seem to be enough to verify the accuracy of developed model.

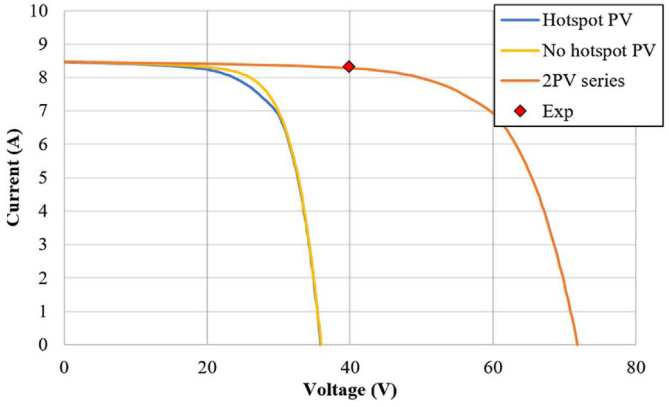

Fig. 9. Comparison of simulation curves for two series connected PV panels (2 P V series) and experimental data (Exp).

4.2. Case 2 – Validation for case local temperature field variations (cooling fins)

This case confirms the model in highly non-uniform temperature field on each cell. The experimental setup thermal camera data is shown in Fig. 12 compared to the numerically obtained data.

For better comparison, the results are compared at two lines in Fig. 13. It can be noticed that the local temperature decrease at the fin-locations correspond to local drops in the experiment. The same intensity of temperature drop is obtained in numerical results. The main advantage of herein shown results is the ability to simulate the small local temperature drops.

4.3. Case 3 – Validation for multiple hot-spot affected cells

The proposed numerical model can also be used on multiple different hot-spot cases. Fig. 14 shows the experimental setup and the corresponding numerical model results.

Possible cause of this hot-spot effect could be dirt accumulation which was insufficiently washed away by summer rain, and thus affected the lower cells. This is a direct type of hot-spot and thus it can be expected that developed model would have some deviations from the experimental data. The hottest cell is still however affected by the indirect hot-spot effect.

Electrical properties for many hot-spot case are presented in Fig. 15.

5. Discussion

The developed model is an efficient tool for analysing behaviour of photovoltaic systems in operating conditions. The model parameters are placed in a manner that they correspond with the panels used in experiment. It needs to be stated however that the material properties given in Table 1 are reported in Ref. [39]. It can be expected that some parameters are improved and this is especially visible on values α, m and V_{br}. When a comparison between studies [38,39] is made differences in values of up to three times can be noticed, and there is approximately 26 years of difference between the papers. In the case of three previously mentioned values, these values are impossible to determine for operating conditions of commercial panel. Thus, the only viable option is to enable the value deviation of ±10% in a more technologically advanced direction. If breakdown voltage V_{br} is reported to be around −15 V for typical pSi cell in 2014 [39] it is presumed that in more modern PV cells this value should be somewhat higher. This way, model can be modified to more accurately correlate with measurement data.

In this research, a photovoltaic panel without parallel connections was used. For 6″ cells, similar to other cell dimensions, open-circuit voltage, V_{OC}, generally ranges from 0.6 V to 0.7 V. Usual commercial solutions of photovoltaic systems may include up to several hundred panels connected in series or in parallel. However, vast majority of stand-alone photovoltaic modules exist with only serial connection. This gives lower current output, but gives higher voltage, and in return produces lower transmission and conversion losses. This model does not cover photovoltaic modules with parallel connections, but with the joining (superposition) of panels' characteristics, model can be utilized for cases of parallelly

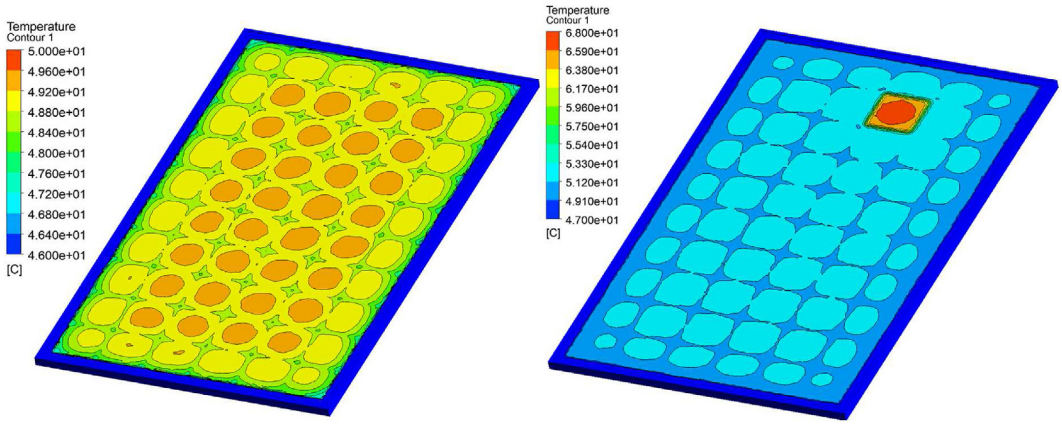

Fig. 10. Top surface PV panel temperature obtained from numerical simulation.

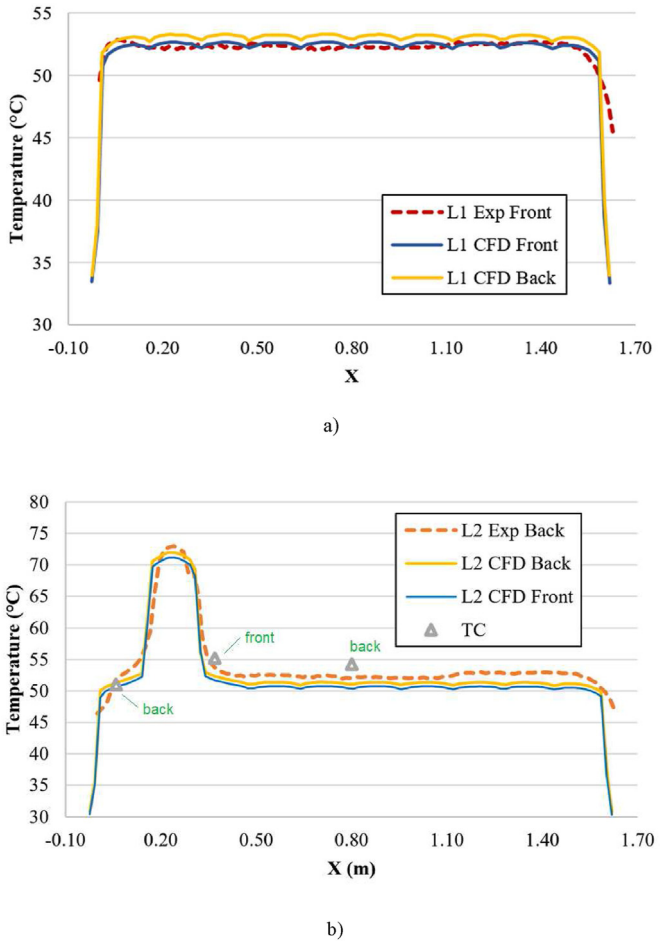

Fig. 11. Comparison of measured and numerical results. Temperature along the surface of PV panel at: a) line L1 and b) Line L2.

connected PV panels.

In Fig. 8, a heating effect from junction box can be noticed. The junction box is not simulated and its effects are not taken into account, and it was not the subject of this research. This however affects the graph results presented in Fig. 11. The issue of junction box is surely interesting, because it is a challenge to distinguish two effects that occur, first one being heating from Joule heat in the conductors, and the second one being thermal insulation on the back side, where junction box acts as an insulator.

The accuracy of the model's quantitative results can and should be discussed. Namely, when measuring in operative conditions, there are too many parameters which cannot be controlled. One such typical parameter is wind velocity. Measurement micro-location is highly susceptible to turbulent wind currents, which makes determination of wind velocity nearly impossible, due to the inertia of measurement equipment. The same goes for total thermal load on the PV panel, since the building envelope (rear wall, behind the panels) seems to be made of anodized metal, with its own distinct reflectivity. The same goes with the building roof, whose reflectivity is surely dependant of incidence angle. This all dictates that a certain degree of error needs to be accepted as reasonable. Therefore, a 1.5 °C of temperature difference between the model and experiment was expected in the first place.

A simple test was made to prove model's sensitivity. By changing the insolation value + - 30 W/m2, it was shown that the temperature at a selected point in any case varies by less than + - 0.6 °C. Thermocouple measurements from the backside show model accuracy of up to 1.5 °C, while thermocouple accuracy is previously stated in Ref. [27] as ± 0.2%.

6. Conclusions

This work investigates a development of thermo-electrical model which takes into account partial hot-spot effect. The model is produced via two-way coupling of electrical model and thermal model, which are produced in MatLab® and ANSYS Fluent (with user defined functions) respectively. Two-way coupling represents the novel approach which has not yet been used in thermo-electrical modelling of hot-spot. Model however has some restrictions, primarily that it covers only partial hot-spot situations for indirect hot-spot. Also, electrical model was developed for serial connection only (since it is the most commonly used).

The developed model was validated via experimental data which is acquired by thermal imaging and temperature sensors. Because of the system complexity an exact matching of modelled and measured results cannot be expected. However, a general temperature change recorded by thermal imaging fit well with numerical data, and temperatures measured by themocouples

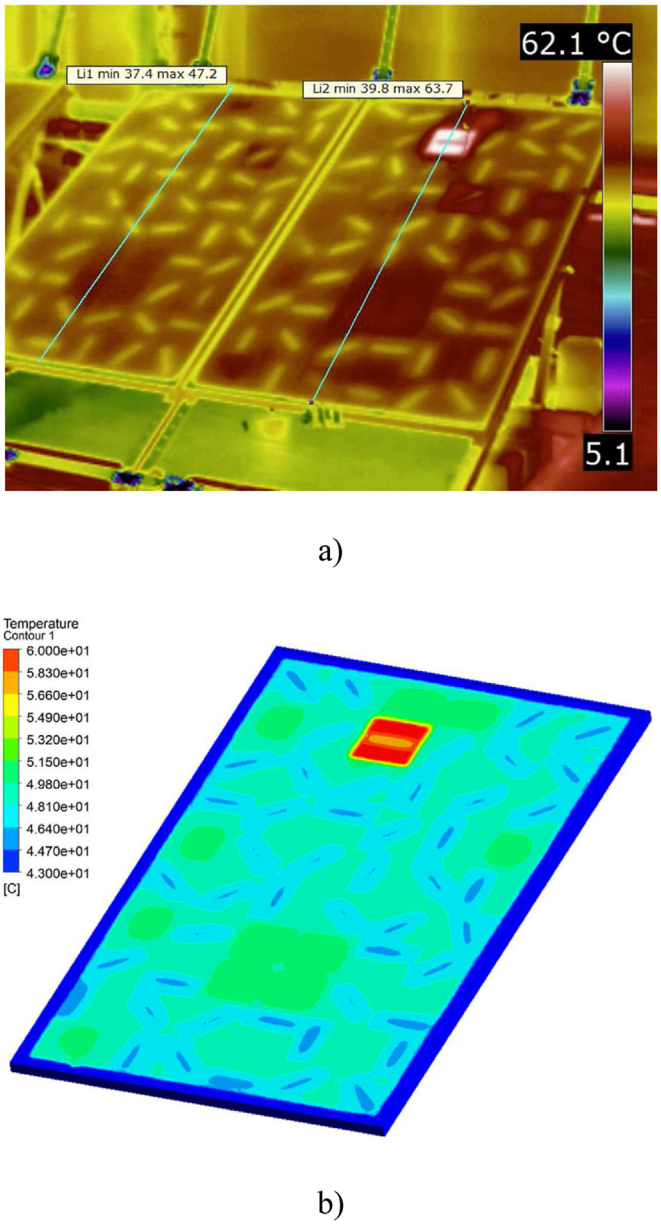

Fig. 12. Comparison of experimental and numerical data: a) thermal imaging of System B and b) Numerical results for the right PV panel.

deviate by less than 1.5 °C from modelled results. Electrical properties of PV panels under partial hot-spot conditions fit with the measured working point of experimental system and which gives confidence in model robustness and usefulness. Additional, sensitivity testing was made and it was shown that there is a reasonable deviation in surface temperature of ±0.6 °C in model results for ±30 W/m^2 of change in solar irradiance. This ±30 W/m^2 difference covers possibilities of inaccurate coefficients implemented in the model, and shows that a temperature difference that occures in model probably stems from inaccuracy of the PV panel coefficients. Herein developed model enables further research work focused on different hot-spot regimes such as influence of hot-spot on global

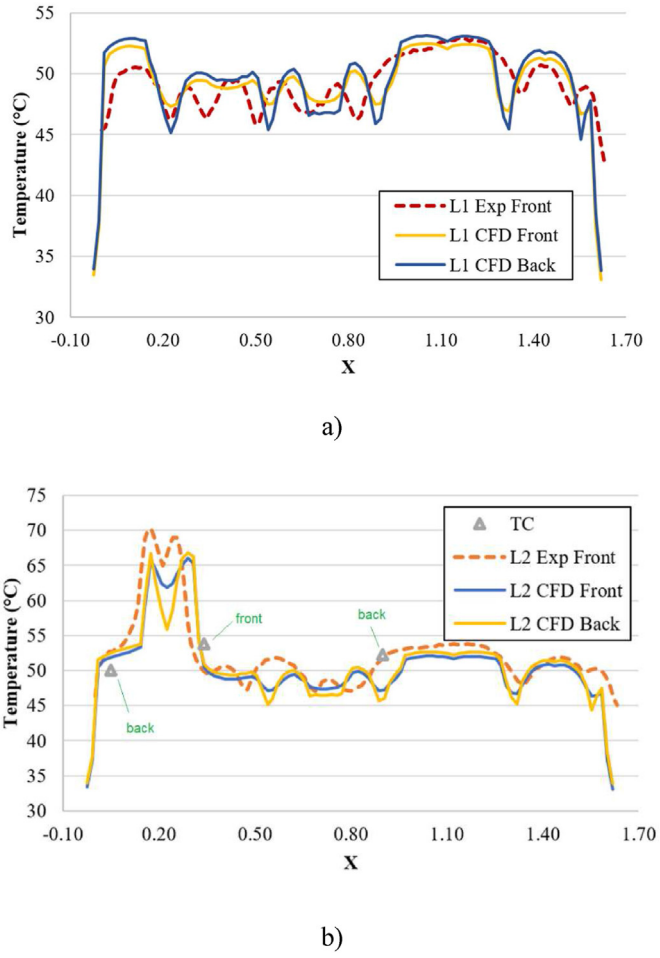

Fig. 13. Comparison of measured and numerical results. Temperature along the surface of PV panel at: a) line L1 and b) Line L2.

efficiency of PV panels from temperature caused efficiency degradation aspect. Moreover, the model can be also used to further optimize bypass diode positioning. The most promising research can be found in potential usage of BIPV (Building Integrated Photovoltaics) hybrid systems, where potentially hot-spot effect can be used to further produce thermal energy if there is necessity. Furthermore, developed model should be upgraded with the direct hot-spot phenomenon, where the cause of hot-spot additionally acts as the heat source on the PV panel surface. Mentioned effect is frequently seen on the PV panels as local dirt accumulation or bird droppings. The current model can easily be updated to consider the local cell-based temperature uniformity effect on the electric model, and thus further to explore the effect of non-uniform cell temperature, which is usually the case with cooled PV panels. Pointwise, the conclusions can be stated as follows:

- 3D model of partial hot-spot effect was developed via two-way coupling and it gives promising results.
- Model is however limited only to partial hot-spot effects, which do not trigger bypass diode.

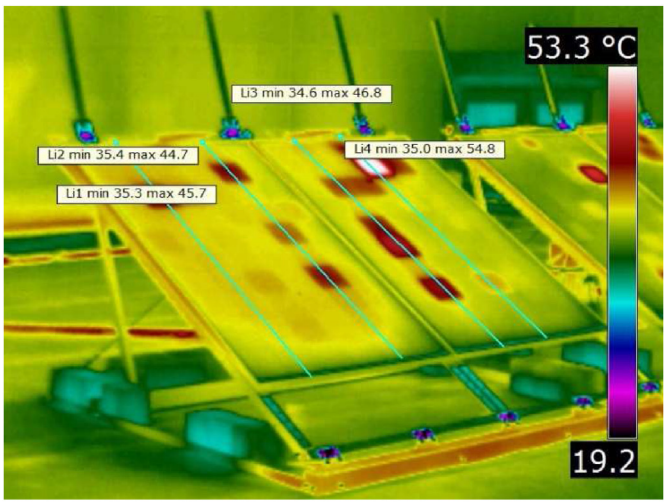

a)

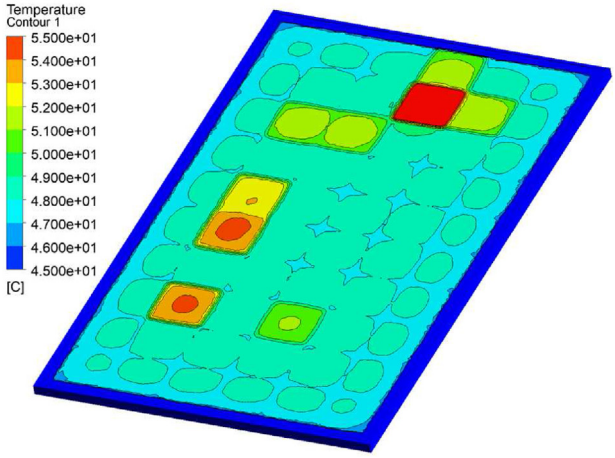

b)

Fig. 14. Qualitative comparison of experimental and numerical data: a) thermal imaging of System B and b) Numerical results for the right PV panel.

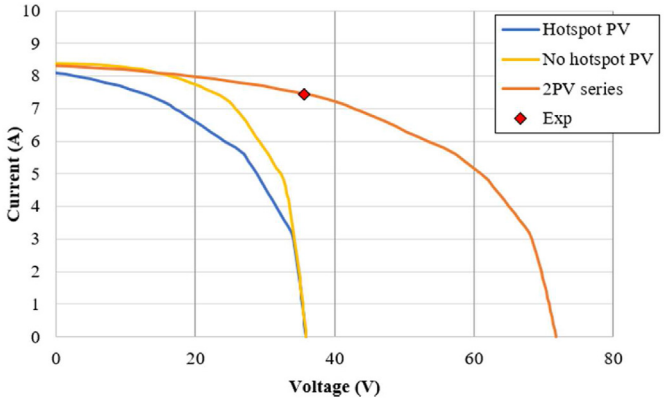

Fig. 15. Electrical characteristics and working point of the system.

- Ideal correlation of numerical and experimental data cannot be expected, deviation of less than 1.5 °C is achieved, which is satisfactory.
- It was shown that the model is robust, since it reacts by a change in ±0.6 °C for ±30 W/m^2 of change in solar irradiance.
- The model adequately covers locally cooled regions, hence it can be used for implementation of cooling techniques for hot-spot mitigation.
- The model adequately covers multi hot-spot situations, so long as the bypass diode is not triggered.

Authors credit statement

Filip Grubišić-Čabo - Conceptualization, Methodology, Analysis of results, Writing, Supervision and Editing. **Ivo Marinić Kragić**; - Conceptualization, Methodology, Analysis of results, Writing. **Tonko Garma** - Methodology, Analysis of results, Writing. **Sandro Nižetić**- Conceptualization, Methodology, Analysis of results, Writing, Supervision and Editing.

Declaration of competing interest

The authors declare that they have no known competing financial interests or personal relationships that could have appeared to influence the work reported in this paper.

Acknowledgments

This work was funded by the Croatian science foundation projects (Research projects: Smart and hybrid cooling techniques for siliceous photovoltaic panels-IP-01-2018-2814 and project Evolutionary optimal shape synthesis with heterogeneous integral and partitined 3D phenotypes, dynamic parameterizations and meshless modelling IP-2018-01-6774).

References

[1] PV magazine n.d. pv-magazine.com/2020/04/06/world-now-has-583-5-gw-of-operational-pv/ (accessed January 20, 2021).
[2] Nhede N. Solar to cover a quarter of global power by 2050 n.d (accessed January 20, 2021), https://www.smart-energy.com/renewable-energy/solar-power-to-cover-a-quarter-of-global-power-by-2050/.
[3] Fraunhofer Institute for Solar Energy Systems n.d. ise.fraunhofer.de/content/dam/ise/de/documents/publications/studies/Photovoltaics-Report.pdf (accessed January 21, 2021).
[4] Nižetić S, Djilali N, Papadopoulos A, Rodrigues JJPC. Smart technologies for promotion of energy efficiency, utilization of sustainable resources and waste management. J Clean Prod 2019;231:565–91. https://doi.org/10.1016/j.jclepro.2019.04.397.
[5] Arndt R, Puto R. Basic understanding of IEC standard testing for photovoltaic panels. 2010.
[6] Skomedal ÅF, Aarseth BL, Haug H, Selj J, Marstein ES. How much power is lost in a hot-spot? A case study quantifying the effect of thermal anomalies in two utility scale PV power plants. Sol Energy 2020. https://doi.org/10.1016/j.solener.2020.10.065.
[7] Kim KA, Krein PT. Photovoltaic hot spot analysis for cells with various reverse-bias characteristics through electrical and thermal simulation. In: 2013 IEEE 14th work. Control model. Power electron, vol. 2013. COMPEL; 2013. https://doi.org/10.1109/COMPEL.2013.6626399.
[8] Bauer J, Wagner JM, Lotnyk A, Blumtritt H, Lim B, Schmidt J, et al. Hot spots in multicrystalline silicon solar cells: avalanche breakdown due to etch pits. Phys Status Solidi Rapid Res Lett 2009. https://doi.org/10.1002/pssr.200802250.
[9] Li Q, Zhu L, Sun Y, Lu L, Yang Y. Performance prediction of Building Integrated Photovoltaics under no-shading, shading and masking conditions using a multi-physics model. Energy 2020. https://doi.org/10.1016/j.energy.2020.118795.
[10] Dhimish M, Holmes V, Mehrdadi B, Dales M, Chong B, Zhang L. Seven indicators variations for multiple PV array configurations under partial shading and faulty PV conditions. Renew Energy 2017. https://doi.org/10.1016/j.renene.2017.06.014.
[11] Dimitrijev S. Understanding semiconductor devices. Oxford: Oxford University Press; 2000.

[12] Giaffreda D, Omaña M, Rossi D, Metra C. Model for thermal behavior of shaded photovoltaic cells under hot-spot condition. Proc. - IEEE Int. Symp. Defect Fault Toler. VLSI Syst. 2011. https://doi.org/10.1109/DFT.2011.47.
[13] Simon M, Meyer EL. Detection and analysis of hot-spot formation in solar cells. Sol Energy Mater Sol Cells 2010. https://doi.org/10.1016/j.solmat.2009.09.016.
[14] Chen S, Weng J, Huang Y, Zhang C, Hu L, Kong F, et al. Numerical model analysis of the shaded dye-sensitized solar cell module. J Phys D Appl Phys 2010. https://doi.org/10.1088/0022-3727/43/30/305102.
[15] Molenbroek E, Waddington DW, Emery KA. Hot spot susceptibility and testing of PV modules. Conf Rec IEEE Photovolt Spec Conf 1992. https://doi.org/10.1109/pvsc.1991.169273.
[16] Xiao WB, Hu FY, Zhang HM, Wu HM. Experimental investigation of the effects of partial shading on photovoltaic cells' electrical parameters. Int J Photoenergy 2015. https://doi.org/10.1155/2015/191603.
[17] Al Mamun MA, Hasanuzzaman M, Selvaraj J. Experimental investigation of the effect of partial shading on photovoltaic performance. IET Renew Power Gener 2017. https://doi.org/10.1049/iet-rpg.2016.0902.
[18] Sharma P, Agarwal V. Maximum power extraction from a partially shaded PV array using shunt-series compensation. IEEE J Photovoltaics 2014. https://doi.org/10.1109/JPHOTOV.2014.2323698.
[19] Deshkar SN, Dhale SB, Mukherjee JS, Babu TS, Rajasekar N. Solar PV array reconfiguration under partial shading conditions for maximum power extraction using genetic algorithm. Renew Sustain Energy Rev 2015. https://doi.org/10.1016/j.rser.2014.10.098.
[20] Prasanth Ram J, Rajasekar N. A new global maximum power point tracking technique for solar photovoltaic (PV) system under partial shading conditions (PSC). Energy 2017. https://doi.org/10.1016/j.energy.2016.10.084.
[21] Farh HMH, Othman MF, Eltamaly AM, Al-Saud MS. Maximum power extraction from a partially shaded PV system using an interleaved boost converter. Energies 2018. https://doi.org/10.3390/en11102543.
[22] Belhaouas N, Cheikh M-SA, Agathoklis P, Oularbi M-R, Amrouche B, Sedraoui K, et al. PV array power output maximization under partial shading using new shifted PV array arrangements. Appl Energy 2017;187:326–37. https://doi.org/10.1016/j.apenergy.2016.11.038.
[23] Ma J, Pan X, Man KL, Li X, Wen H, On Ting T. Detection and assessment of partial shading scenarios on photovoltaic strings. IEEE Trans Ind Appl 2018. https://doi.org/10.1109/TIA.2018.2848643.
[24] Du D, Darkwa J, Kokogiannakis G. Thermal management systems for Photovoltaics (PV) installations: a critical review. Sol Energy 2013;97:238–54. https://doi.org/10.1016/j.solener.2013.08.018.
[25] Popovici CGCG, Hudişteanu SV, Mateescu TD, Cherecheş N-CC. Efficiency improvement of photovoltaic panels by using air cooled heat sinks. Energy Procedia 2016;85:425–32. https://doi.org/10.1016/j.egypro.2015.12.223.
[26] Nižetić S, Grubišić- Čabo F, Marinić-Kragić I, Papadopoulos AM. Experimental and numerical investigation of a backside convective cooling mechanism on photovoltaic panels. Energy 2016;111:211–25. https://doi.org/10.1016/j.energy.2016.05.103.
[27] Grubišić-Čabo F, Nižetić S, Marinić Kragić I, Čoko D. Further progress in the research of fin-based passive cooling technique for the free-standing silicon photovoltaic panels. Int J Energy Res 2019;43. https://doi.org/10.1002/er.4489.
[28] Grubišić-Čabo F, Nižetić S, Čoko D, Marinić Kragić I, Papadopoulos A. Experimental investigation of the passive cooled free-standing photovoltaic panel with fixed aluminum fins on the backside surface. J Clean Prod 2018;176. https://doi.org/10.1016/j.jclepro.2017.12.149.
[29] Hasanuzzaman M, Malek ABM, Islam MMM, Pandey AKK, Rahim NAA. Global advancement of cooling technologies for PV systems: a review. Sol Energy 2016;137:25–45. https://doi.org/10.1016/j.solener.2016.07.010.
[30] Marinić-Kragić I, Nižetić S, Grubišić-Čabo F, Papadopoulos AM. Analysis of flow separation effect in the case of the free-standing photovoltaic panel exposed to various operating conditions. J Clean Prod 2018;174. https://doi.org/10.1016/j.jclepro.2017.10.310.
[31] Bahaidarah HMS, Baloch AAB, Gandhidasan P. Uniform cooling of photovoltaic panels: a review. Renew Sustain Energy Rev 2016;57:1520–44. https://doi.org/10.1016/j.rser.2015.12.064.
[32] Royne A, Dey CJ, Mills DR. Cooling of photovoltaic cells under concentrated illumination: a critical review. Sol Energy Mater Sol Cells 2005. https://doi.org/10.1016/j.solmat.2004.09.003.
[33] Rossi D, Omana M, Giaffreda D, Metra C. Modeling and detection of hotspot in shaded photovoltaic cells. IEEE Trans Very Large Scale Integr Syst 2015. https://doi.org/10.1109/TVLSI.2014.2333064.
[34] Baloch AAB, Bahaidarah HMS, Gandhidasan P, Al-Sulaiman FA. Experimental and numerical performance analysis of a converging channel heat exchanger for PV cooling. Energy Convers Manag 2015;103:14–27. https://doi.org/10.1016/j.enconman.2015.06.018.
[35] Olukan TA, Emziane M. A comparative analysis of PV module temperature models. Energy Procedia 2014;62:694–703. https://doi.org/10.1016/j.egypro.2014.12.433.
[36] Acharya P, Shaikh MN, Jha SK, Papadakis AP. Electrical modelling of a photovoltaic module. 2016. https://doi.org/10.22618/TP.EI.20163.389014.
[37] Msirdi N, K M'sirdi N, Benabdellatif M, Tina GM, Naamane A. Dynamic coupled electrical and thermal model for PV-T solar energy collectors. In: EFEA. vol. 2018; 2018. Valencia, Spain.
[38] Bishop JW. Computer simulation of the effects of electrical mismatches in photovoltaic cell interconnection circuits. Sol Cell 1988. https://doi.org/10.1016/0379-6787(88)90059-2.
[39] Díaz-Dorado E, Cidrás J, Carrillo C. Discrete I-V model for partially shaded PV-arrays. Sol Energy 2014. https://doi.org/10.1016/j.solener.2014.01.037.
[40] Khatib T, Elmenreich W. Modeling of photovoltaic systems using MATLAB ®. Hoboken, NJ, USA: John Wiley & Sons, Inc.; 2016. https://doi.org/10.1002/9781119118138.index.
[41] Honsberg CB, Bowden SG. Photovoltaics education website n.d. www.pveducation.org.
[42] Kitamura R, Pilon L, Jonasz M. Optical constants of silica glass from extreme ultraviolet to far infrared at near room temperature. Appl Opt 2007. https://doi.org/10.1364/AO.46.008118.
[43] ANSYS Inc. ANSYS (computer program). 2020.
[44] Jubayer CM, Siddiqui K, Hangan H. CFD analysis of convective heat transfer from ground mounted solar panels. Sol Energy 2016;133:556–66. https://doi.org/10.1016/j.solener.2016.04.027.
[45] Zhu L, Raman A, Wang KX, Anoma MA, Fan S. Radiative cooling of solar cells. Optica 2014;1:32. https://doi.org/10.1364/OPTICA.1.000032.
[46] IEC Standard. 61215 crystalline silicon terrestrial photovoltaic (PV) modules design qualification and type approval 1983.